

Spin transfer torque enhancement in dual spin valve in the ballistic regime

P. Yan,¹ Z. Z. Sun,² and X. R. Wang¹

¹*Physics Department, The Hong Kong University of Science and Technology, Clear Water Bay, Hong Kong SAR, China*

²*Institute for Theoretical Physics, University of Regensburg, D-93040 Regensburg, Germany*

(Dated: November 8, 2018)

The spin transfer torque in all-metal dual spin valve, in which two antiparallely aligned pinned ferromagnetic layers are on the two sides of a free ferromagnetic layer with two thin nonmagnetic spacers in between, is studied in the ballistic regime. It is argued that, similar to the results in the diffusion regime, the spin transfer torque is dramatically enhanced in comparison to that in a conventional spin valve although no spin accumulation exists at the magnetic-nonmagnetic interfaces. Within the Slonczewski's approach, an analytical expression of the torque on the free magnetic layer is obtained, which may serve as a theoretical model for the micromagnetic simulation of the spin dynamics in dual spin valve. Depending on the orientation of free layer and the degree of electron polarization, the spin transfer torque enhancement could be tens times. The general cases when transmission and reflection probabilities of free layer are different from zero or one are also numerically calculated.

PACS numbers: 72.25.Ba, 75.60.Jk, 85.70.Ay, 85.75.-d

I. INTRODUCTION

Current induced magnetization reversal of magnetic multilayers has attracted much research interest due to its rich physics and potential applications in spintronic devices.¹⁻⁸ Spin valve, consisting of two ferromagnetic layers and one nonmagnetic spacer in between, is one of such multilayer structures. In a spin valve, one of the magnetic layers, acting as a spin polarizer, is thick so that conducting electrons are polarized after passing through it. The polarized conducting electrons will transfer their spin angular momentums to local magnetization of the thinner free magnetic layer, resulting in the spin transfer torque (STT) effect first proposed by Slonczewski⁹ and Berger.¹⁰ Although the STT has many advantages over a magnetic field in manipulating magnetization state,^{11,12} a large current density is needed to achieve a technologically useful magnetization switching speed,^{13,14} but the associated Joule heating could affect device performance. Therefore, the current density reduction becomes a challenging issue from the spintronics application viewpoint.¹⁵

Many efforts have been devoted to the issue, including using optimized time-dependent current pulse,¹⁶ pure spin current,¹⁷ and thermal activation.^{18,19} One direct approach is to increase the magnitude of the STT under a given current through unique geometry design. In 2003, Berger²⁰ proposed a novel magnetic multilayer architecture called dual spin valve (DSV) where the free magnetic layer is sandwiched between two thicker pinned magnetic layers with opposite magnetizations. It is predicted that the STT applied on the free magnetic layer should be much larger than that in a traditional spin valve for a given current in the diffusion regime.²⁰ The argument is that spins accumulate at both non-magnetic/magnetic interfaces of the free layer and STT is proportional to spin accumulations.²⁰ However, it is not clear whether this STT enhancement can occur in DSV in the ballistic

regime without spin accumulations. Moreover, the analytical formalism for the STT in DSV is still an open problem up to now.^{21,22} These are the focuses of present paper. A full-quantum description of the STT, valid when both the mean-free path and the spin-flip relaxation length are larger than the thickness of the spacers, is presented. Averaged (over electron phases) STT is obtained analytically within the Slonczewski's semiclassical approach⁹ when all magnetic layers are perfect polarizers. It is found that STT in DSV, depending on the orientation of free layer and the degree of electron polarization, can be enhanced by a factor of tens in comparison with that in a spin valve. The general cases of arbitrary transmission and reflection coefficients of free layer are also numerically calculated.

This paper is organized as follows: In Sec. II, a physical picture of STT origin in both spin valve and DSV is presented. Sec. III is the theoretical model and formulation of the electron transport through a DSV. The results, including the analytical expression of the STT on the free layer within the Slonczewski approach, are given in Sec. IV. Sec. V is the summary.

II. PHYSICAL PICTURE

It shall be useful to present first a physical picture about STT origin in spin valve and, in particular, its enhancement in DSV. Consider a spin valve, which is schematically shown in Fig. 1(a), consisting of a pinned ferromagnetic layer FM_A and a free ferromagnetic layer FM_B separated by a nonmagnetic spacer NM. The magnetizations of FM_A and FM_B are represented by unit vectors, \mathbf{m}_A and \mathbf{m}_B , and their saturated magnetizations. For the simplicity, we assume that both ferromagnetic layers are perfect spin filters, such that spins aligned parallelly with the layer magnetization can completely transmit through the layer, while antiparallel spins are totally

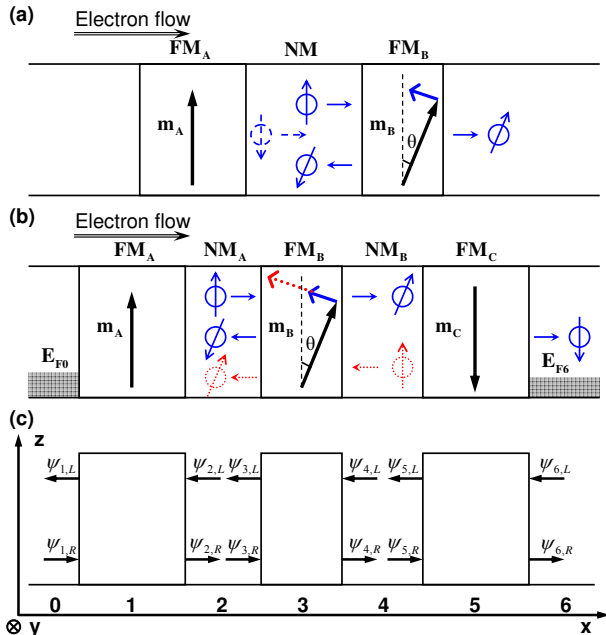


FIG. 1: (Color online) (a) Illustration of STT generated in spin valve. The circles with arrows illustrate the electron flow with spin polarization direction. (b) Schematic explanation of STT enhancement in DSV. $V_b = E_{F0} - E_{F6}$ is the applied bias. $FM_{A,B,C}$ are ferromagnetic layers and $NM_{A,B}$ are nonmagnetic layers. (c) Wave functions at the interfaces of regions (0 – 6) in DSV and the coordinates orientation.

reflected. In this ideal case, a closed analytical solution of the STT can be obtained, which will be shown later.

Consider electrons flowing from the left to the right in Fig. 1(a). The right-going electrons are initially polarized along \mathbf{m}_A direction after passing through FM_A . They will remain their spin polarization when they impinge on FM_B , as long as the spacer thickness is much shorter than the spin-diffusion length, which is usually the case in nanoscale spin valves. Because the polarization direction of FM_B is noncollinear with that of FM_A , an electron polarized along \mathbf{m}_A is the superposition of two states along \mathbf{m}_B and $-\mathbf{m}_B$, so that the component along \mathbf{m}_B can transmit through FM_B while that along $-\mathbf{m}_B$ is totally reflected since FM_B is a perfect polarizer. Thus, there will be a net angular momentum transfer, perpendicular to \mathbf{m}_B , from impinged electrons to FM_B , resulting in a torque on FM_B to align its magnetization toward \mathbf{m}_A , as shown by the blue arrow in Fig. 1(a). This is the origin of STT in spin valve. It should be pointed out that the subsequent multiple reflections of electrons within the NM spacer by the two FM/NM interfaces will reduce the STT, since the reflected electrons (dashed symbols in Fig. 1(a)) from FM_B to FM_A and back to FM_B will exert a torque along $-\mathbf{m}_A$. However, the net torque will not be zero since the reflected electrons have smaller flux than that of the original injected electrons.

Let us now examine the spin transfer in a DSV shown

in Fig. 1(b). On the top of a usual spin valve (Fig. 1(a)), an additional pinned ferromagnetic layer FM_C with an antiparallely aligned magnetization to FM_A , i.e., $\mathbf{m}_C = -\mathbf{m}_A$, is added so that the free layer FM_B is now sandwiched between FM_A and FM_C , separated by two nonmagnetic spacers NM_A and NM_B , respectively. Similar to the case of a spin valve, right-going electrons transmitting through FM_A will exert a STT on FM_B to align \mathbf{m}_B with \mathbf{m}_A , as shown by the blue arrow in Fig. 1(b). After the electrons transmit through FM_B , most of them will be reflected by FM_C and then impinge again on FM_B , as shown by red-dashed symbols in Fig. 1(b). Thus, they will exert another STT on FM_B along $-\mathbf{m}_C = \mathbf{m}_A$ direction, resulting in the STT enhancement. Multiple reflections in region 2 (Fig. 1(c)) tend to reduce the torque but will not cancel it totally. In the following sections we will verify this physical picture through a full-quantum mechanics calculation.

III. MODEL AND FORMULATION

Single charge and spin transport theory in magnetic multilayers was well developed and approaches vary from classical Valet-Fert theory in the diffusive regime,²³ matrix Boltzmann equation formalism,²⁴ to full-quantum mechanical treatments.^{9,25–30} In the present paper, we will adopt a full-quantum mechanical description called scattering matrix method^{28–30} that is valid for ballistic transmission. We assume that interfaces are flat and clean and all spin-flip processes are negligible so that momentum \mathbf{k} is a good quantum number in each layer. Wavefunction at the interface of layers labeled by $n = 1 - 6$ as shown in Fig. 1(c) can be written as a two-component spinor multiplied by spatial plane wave,

$$\psi_{n,\alpha}(x) = \begin{pmatrix} \chi_{n,\alpha,\uparrow} \\ \chi_{n,\alpha,\downarrow} \end{pmatrix} e^{ix(k_x)_{n,\alpha}}, \quad (1)$$

where α denotes propagation directions, $\alpha = L$ for leftward and $\alpha = R$ for rightward. k_x is the x -component of wave vector. $\chi_{n,\alpha,\uparrow(\downarrow)}$ is the spin-up (-down) probability amplitude. z -axis is along \mathbf{m}_A . \mathbf{m}_B is specified by a polar angle θ and an azimuthal angle ϕ .

Incoming and outgoing spinor states in each region are connected to each other by a scattering matrix.^{28–30} In region n ($= 1, 2, 3, 4, 5$), $\psi_{n,L}$ and $\psi_{n+1,R}$ are outgoing spinors while $\psi_{n,R}$ and $\psi_{n+1,L}$ are incoming spinors. They relate to each other by a scattering matrix \hat{S}_n ,

$$\begin{pmatrix} \psi_{n,L} \\ \psi_{n+1,R} \end{pmatrix} = \hat{S}_n \begin{pmatrix} \psi_{n,R} \\ \psi_{n+1,L} \end{pmatrix}. \quad (2)$$

Note that $\psi_{6,L} = 0$ since electrons flow from the left reservoir to the right one. \hat{S}_n is a 4×4 matrix and can be expressed by transmission and reflection coefficients of each scattering region,

$$\hat{S}_n = \begin{pmatrix} \hat{r}_n & \hat{t}_n \\ \hat{t}_n & \hat{r}_n \end{pmatrix}, \quad (3)$$

where \hat{t}_n (\hat{r}_n) with $n = 1, 2, 3, 4, 5$ are 2×2 transmission (reflection) matrices for layers FM_A , NM_A , FM_B , NM_B , and FM_C , respectively.

We will first treat the pinned ferromagnetic layers FM_A and FM_C as perfect polarizers. Hence \hat{t}_1 , \hat{r}_1 , \hat{t}_5 , and \hat{r}_5 take the following forms

$$\hat{t}_1 = \hat{r}_5 = \begin{pmatrix} 1 & 0 \\ 0 & 0 \end{pmatrix}, \quad \hat{r}_1 = \hat{t}_5 = \begin{pmatrix} 0 & 0 \\ 0 & 1 \end{pmatrix}. \quad (4)$$

Since there is no scatterings in nonmagnetic layers NM_A and NM_B and the propagation of electrons in these layers accumulate dynamical phases, we have

$$\hat{t}_2 = \exp(i\varphi_A) \hat{I}, \quad \hat{t}_4 = \exp(i\varphi_B) \hat{I}, \quad \hat{r}_2 = \hat{r}_4 = 0, \quad (5)$$

where φ_A and φ_B are the corresponding phase shifts and \hat{I} is the 2×2 unit matrix. The scattering matrix for FM_B can be expressed by the angles θ and ϕ as

$$\begin{aligned} \hat{t}_3 &= \hat{R}(\theta, \phi) \mathbf{t} \hat{R}^{-1}(\theta, \phi), \\ \hat{r}_3 &= \hat{R}(\theta, \phi) \mathbf{r} \hat{R}^{-1}(\theta, \phi), \end{aligned} \quad (6)$$

where $\hat{R}(\theta, \phi)$ is the rotation that brings \hat{z} into \mathbf{m}_B ,

$$\hat{R} = e^{-\frac{i\phi}{2}\sigma_z} e^{-\frac{i\theta}{2}\sigma_y} = \begin{pmatrix} e^{-\frac{i\phi}{2}} \cos \frac{\theta}{2} & -e^{-\frac{i\phi}{2}} \sin \frac{\theta}{2} \\ e^{\frac{i\phi}{2}} \sin \frac{\theta}{2} & e^{\frac{i\phi}{2}} \cos \frac{\theta}{2} \end{pmatrix}. \quad (7)$$

\mathbf{t} and \mathbf{r} are the transmission and reflection matrices when \mathbf{m}_B is chosen as the quantization axis

$$\mathbf{t} = \begin{pmatrix} t_u & 0 \\ 0 & t_d \end{pmatrix}, \quad \mathbf{r} = \begin{pmatrix} r_u & 0 \\ 0 & r_d \end{pmatrix}, \quad (8)$$

where t_u , t_d , r_u , and r_d are transmission and reflection parameters. Subscripts u and d stand for spin-up (majority) and spin-down (minority), respectively. These parameters are complex numbers in general. $t_u = 1$, $t_d = 0$ and $r_u = 0$, $r_d = 1$ if FM_B is a perfect polarizer.

To find the STT on free layer FM_B , we need to obtain the scattering states at the two interfaces of FM_B . The spin-dependent scattering wave functions can be expressed in terms of incoming wave $\psi_{1,R}$, such as $\psi_{n,\alpha} = \hat{P}_{n,\alpha} \psi_{1,R}$ ($n = 3, 4, 6$), where matrices $\hat{P}_{n,\alpha}$ are given by

$$\begin{aligned} \hat{P}_{3,R} &= \left[\left(\hat{I} - \hat{t}_2^2 \hat{r}_1 \hat{r}_3 \right) - \hat{t}_2^2 \hat{t}_4^2 \hat{r}_1 \hat{t}_3 \hat{r}_5 \left(\hat{I} - \hat{t}_4^2 \hat{r}_3 \hat{r}_5 \right)^{-1} \hat{t}_3 \right]^{-1} \\ &\quad \hat{t}_2 \hat{t}_1, \\ \hat{P}_{3,L} &= \hat{r}_3 \hat{P}_{3,R} + \hat{t}_4 \hat{t}_3 \hat{r}_5 \hat{Q}, \\ \hat{P}_{4,R} &= \hat{t}_4^{-1} \hat{Q}, \quad \hat{P}_{4,L} = \hat{t}_4 \hat{r}_5 \hat{Q}, \\ \hat{P}_{6,R} &= \hat{t}_5 \hat{Q}, \end{aligned} \quad (9)$$

with

$$\begin{aligned} \hat{Q} &= \left[\left(\hat{I} - \hat{t}_4^2 \hat{r}_3 \hat{r}_5 \right) - \hat{t}_2^2 \hat{t}_4^2 \hat{t}_3 \left(\hat{I} - \hat{t}_2^2 \hat{r}_1 \hat{r}_3 \right)^{-1} \hat{r}_1 \hat{t}_3 \hat{r}_5 \right]^{-1} \\ &\quad \hat{t}_3 \left(\hat{I} - \hat{t}_2^2 \hat{r}_1 \hat{r}_3 \right)^{-1} \hat{t}_2 \hat{t}_4 \hat{t}_1. \end{aligned} \quad (10)$$

After some algebras, we have

$$\hat{Q} = \frac{\sqrt{z_1 z_2}}{D(z_1, z_2)} \begin{bmatrix} Q^{\uparrow\uparrow}(z_1, z_2) & 0 \\ Q^{\downarrow\uparrow}(z_1, z_2) & 0 \end{bmatrix}, \quad (11a)$$

$$\hat{P}_{3,R} = \frac{\sqrt{z_1}}{D(z_1, z_2)} \begin{bmatrix} P_{3,R}^{\uparrow\uparrow}(z_1, z_2) & 0 \\ P_{3,R}^{\downarrow\uparrow}(z_1, z_2) & 0 \end{bmatrix}, \quad (11b)$$

$$\hat{P}_{3,L} = \frac{\sqrt{z_1}}{D(z_1, z_2)} \begin{bmatrix} P_{3,L}^{\uparrow\uparrow}(z_1, z_2) & 0 \\ P_{3,L}^{\downarrow\uparrow}(z_1, z_2) & 0 \end{bmatrix}, \quad (11c)$$

$$\hat{P}_{4,R} = \frac{\sqrt{z_1}}{D(z_1, z_2)} \begin{bmatrix} Q^{\uparrow\uparrow}(z_1, z_2) & 0 \\ Q^{\downarrow\uparrow}(z_1, z_2) & 0 \end{bmatrix}, \quad (11d)$$

$$\hat{P}_{4,L} = \frac{z_2 \sqrt{z_1}}{D(z_1, z_2)} \begin{bmatrix} Q^{\uparrow\uparrow}(z_1, z_2) & 0 \\ 0 & 0 \end{bmatrix}, \quad (11e)$$

where $z_1 = \exp(i2\varphi_A)$, $z_2 = \exp(i2\varphi_B)$, and

$$\begin{aligned} Q^{\uparrow\uparrow}(z_1, z_2) &= t_u \cos^2 \frac{\theta}{2} + t_d \sin^2 \frac{\theta}{2} \\ &- z_1 \left(r_d t_u \cos^2 \frac{\theta}{2} + r_u t_d \sin^2 \frac{\theta}{2} \right), \end{aligned} \quad (12a)$$

$$\begin{aligned} Q^{\downarrow\uparrow}(z_1, z_2) &= \frac{1}{2} e^{i\phi} \sin \theta \left[t_u - t_d \right. \\ &+ (z_1 + z_2) (r_u t_d - r_d t_u) \\ &\left. + z_1 z_2 (t_u r_d^2 + t_d t_u^2 - t_u t_d^2 - t_d r_u^2) \right], \end{aligned} \quad (12b)$$

$$\begin{aligned} D(z_1, z_2) &= 1 - z_1 \left(r_u \sin^2 \frac{\theta}{2} + r_d \cos^2 \frac{\theta}{2} \right) \\ &- z_2 \left(r_u \cos^2 \frac{\theta}{2} + r_d \sin^2 \frac{\theta}{2} \right) + \end{aligned} \quad (12c)$$

$$\begin{aligned} &z_1 z_2 \left[r_u r_d + \frac{\sin^2 \theta}{4} \left((r_u - r_d)^2 - (t_u - t_d)^2 \right) \right], \\ P_{3,R}^{\uparrow\uparrow}(z_1, z_2) &= D(z_1, z_2), \end{aligned} \quad (12d)$$

$$\begin{aligned} P_{3,R}^{\downarrow\uparrow}(z_1, z_2) &= \frac{1}{2} z_1 e^{i\phi} \sin \theta \left[r_u - r_d \right. \\ &+ z_2 (-r_u^2 + r_u r_d + t_u^2 - t_u t_d) \cos^2 \frac{\theta}{2} \end{aligned} \quad (12e)$$

$$\begin{aligned} &+ z_2 (r_d^2 - r_u r_d - t_d^2 + t_u t_d) \sin^2 \frac{\theta}{2} \left. \right], \\ P_{3,L}^{\uparrow\uparrow}(z_1, z_2) &= z_2 \left(t_u \cos^2 \frac{\theta}{2} + t_d \sin^2 \frac{\theta}{2} \right)^2 \end{aligned}$$

$$\begin{aligned} &- z_2 \left(r_u \cos^2 \frac{\theta}{2} + r_d \sin^2 \frac{\theta}{2} \right)^2 \\ &+ r_u \cos^2 \frac{\theta}{2} + r_d \sin^2 \frac{\theta}{2} \end{aligned} \quad (12f)$$

$$+ z_1 z_2 \left[r_u (r_d^2 - t_d^2) \sin^2 \frac{\theta}{2} + r_d (r_u^2 - t_u^2) \cos^2 \frac{\theta}{2} \right],$$

$$P_{3,L}^{\downarrow\uparrow}(z_1, z_2) = \frac{P_{3,R}^{\downarrow\uparrow}(z_1, z_2)}{z_1}. \quad (12g)$$

The notation $X^{\downarrow\uparrow}$ ($X = \hat{Q}, \hat{P}_{3,R}, \hat{P}_{3,L}$) refers to the transition amplitude from spin-up to spin-down states.

IV. RESULTS AND DISCUSSIONS

A. Charge current

An applied bias V_b shown in Fig. 1(b) generates a charge current J_e and a spatially dependent spin current \mathbf{J}_s through the device. At zero temperature, the charge current reads

$$J_e = \int dE \sum_{\mathbf{q}} j_e(\mathbf{q}), \quad (13)$$

with charge current density

$$j_e(\mathbf{q}) = e \frac{\hbar k_x}{m} \psi_{6,R}^\dagger \psi_{6,R}, \quad (14)$$

where \mathbf{q} is the transverse wave vector with energy E , $k_x^2 + \mathbf{q}^2 = 2mE/\hbar^2$, and e , m , \hbar are the electron charge, electron mass and the Planck constant. The charge current density can also be written as

$$j_e = e \frac{\hbar k_x}{m} T_e(z_1, z_2), \quad (15)$$

with transmission coefficient

$$T_e(z_1, z_2) = \frac{|Q^{\downarrow\uparrow}(z_1, z_2)|^2}{|D(z_1, z_2)|^2}. \quad (16)$$

In the case that electrons propagate ballistically through NM_A and NM_B , the phase shifts in normal metals are given by $\varphi_A = k_x l_A$ and $\varphi_B = k_x l_B$ where l_A and l_B are the widths of NM_A and NM_B , respectively. For sufficiently thick (much bigger than electron Fermi wave length but still smaller than the spin diffusion length) NM layers, φ_A and φ_B vary rapidly from state to state. Thus, when one sums up contributions from different electronic states (different k_x), it is justifiable to assume φ_A and φ_B to be random,²⁹ and $z_1 = \exp(i2\varphi_A)$ and $z_2 = \exp(i2\varphi_B)$ are equally distributed on the unit circle of the complex plane.^{28,29} However, one should note that z_1 and z_2 are not independent under the ballistic assumption since $z_2 = (z_1)^p$ with $p = l_B/l_A$. The average transmission coefficient is then

$$\begin{aligned} \langle T_e \rangle &= \frac{1}{\pi} \int_0^\pi T_e(\varphi_A, p\varphi_A) d\varphi_A \\ &= \frac{1}{2\pi i} \oint_C \frac{T_e(z_1, (z_1)^p)}{z_1} dz_1, \end{aligned} \quad (17)$$

where C is contour $|z_1| = 1$. The contour integral for $p = 1$, corresponding to the symmetric DSV configuration,^{22,31} is

$$\langle T_e \rangle = \sum_{l=1}^s \text{Res} \left(\frac{T_e(z_1)}{z_1}; z_{1,l} \right), \quad (18)$$

where $z_{1,l}$ is the l -th pole of function $T_e(z_1)/z_1$ and s is the total number of poles inside the unit circle. In case

when FM_B is perfect, i.e., $t_u = 1$ and $t_d = 0$ ($r_u = 0$, and $r_d = 1$), function $T_e(z_1)/z_1$ has only a second-order pole $z_1 = 0$ inside the unit circle. Thus, we can get the average transmission

$$\langle T_e \rangle (t_u = 1, t_d = 0) = \frac{\sin^2 \theta}{2}. \quad (19)$$

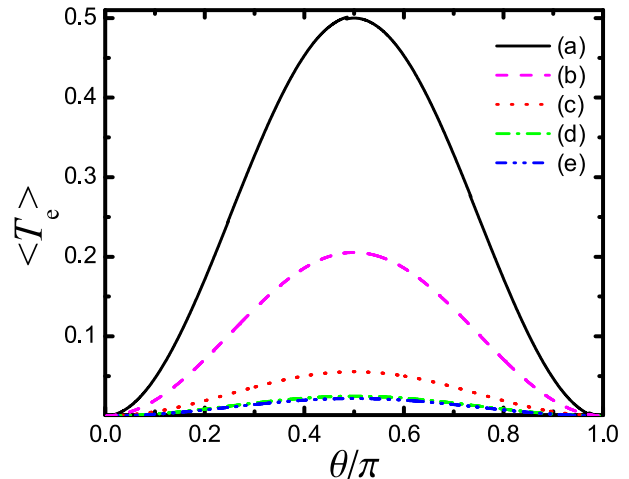


FIG. 2: (Color online) Average transmission coefficient versus angle θ for (a) $t_u = 1$ and $t_d = 0$; (b) $|t_u|^2 = 0.84$ and $|t_d|^2 = 0.17$; (c) $|t_u|^2 = 0.79$ and $|t_d|^2 = 0.49$; (d) $|t_u|^2 = 0.66$ and $|t_d|^2 = 0.44$; and (e) $|t_u|^2 = 0.73$ and $|t_d|^2 = 0.54$.

Figure 2 is the average transmission coefficient versus angle θ for (a) perfect polarizers; (b) (001) interface of Au/Fe; (c) (001) interface of Cu/Co; (d) (110) interface of Cu/Co; (e) (111) interface of Cu/Co. The model parameters for (b-e) are obtained from Ref. 32, where they were extracted from the first-principles calculations. All transmission and reflection amplitudes are assumed to be real. We find that the average total transmission approach zero as θ goes to 0 or π even if t_d is finite for the minority electrons, which is different from the result (Fig. 3 in Ref. 28) in traditional spin valve. The reasons are as follows. For $\theta = 0$, all electrons are polarized along \mathbf{m}_A after passing through FM_B . They will be totally reflected by FM_C because of $\mathbf{m}_C = -\mathbf{m}_A$, leading to zero electric current. On the other hand, for $\theta = \pi$, all electrons that transmit FM_A will be completely reflected by FM_B if it is a perfect polarizer because electron spins are antiparallel to \mathbf{m}_B , while electrons passing through FM_B will maintain polarization along \mathbf{m}_A in the case of $t_d \neq 0$ and they will be totally reflected by FM_C because of $\mathbf{m}_C = -\mathbf{m}_A$. Hence, the average transmission in DSV vanishes at $\theta = 0$ or π .

The total charge current flowing through the DSV can be obtained by summing Eq. (15) over the transverse momentum \mathbf{q} . To find an analytical expression, we will adopt the semiclassical Slonczewski approach.⁹ Within the Stoner description of magnetism and let Δ be the exchange energy of two spin bands of FM_B , one can define

two Fermi wave vectors K_+ and K_- for majorities and minorities,

$$K_+ = \sqrt{2mE/\hbar^2}, \quad K_- = \sqrt{2m(E - \Delta)/\hbar^2}. \quad (20)$$

For a ferromagnetic metal, we assume that the Fermi energy lies above the exchange potential, and electrons in NMs are ideally matched with the majority electrons in FM, i.e., $k = K_+$. The possible momentum states that contribute to the current can be divided into three ranges.^{9,28}

Range a: $0 \leq q < K_-$. Electrons of both spins in these states contribute to charge current J_a ,

$$\begin{aligned} J_a &= 2e \frac{\hbar}{(2\pi)^2 m} \int_0^{K_-} \sqrt{K_+^2 - q^2} q dq \\ &= \frac{2}{3} e \frac{\hbar}{(2\pi)^2 m} \left[(K_+^2)^{3/2} - (K_+^2 - K_-^2)^{3/2} \right]. \end{aligned} \quad (21)$$

Range b: $K_- \leq q < K_+$. Only majority spin electrons contribute to current J_b ,

$$\begin{aligned} J_b &= e \frac{\hbar}{(2\pi)^2 m} \int_{K_-}^{K_+} \sqrt{K_+^2 - q^2} q dq \\ &= \frac{1}{3} e \frac{\hbar}{(2\pi)^2 m} (K_+^2 - K_-^2)^{3/2}. \end{aligned} \quad (22)$$

Range c: $K_+ \leq q$. All electrons are totally reflected, and there is no charge current flow, i.e., $J_c = 0$.

Using the conventional definition of spin polarization

$$P = \frac{n_+ - n_-}{n_+ + n_-} = \frac{K_+ - K_-}{K_+ + K_-}, \quad (23)$$

where n_{\pm} are the majority/minority spin densities at Fermi level in the FMs, the ratio J_a/J_b can be written as a function of polarization P ,

$$\frac{J_a}{J_b} = \frac{(1+P)^3}{4P^{3/2}} - 2. \quad (24)$$

Note that J_b is the maximal polarized current for parallel FMs configuration. Then, to get the total charge current, it should be multiplied by the average transmission coefficient. Thus, the total electron current is given by^{9,28}

$$J_e = J_a + \langle T_e \rangle J_b. \quad (25)$$

B. Spin current and spin transfer torque

The spin currents on two sides of FM_B are

$$\mathbf{J}_{3s} = \int dE \sum_{\mathbf{q}} \mathbf{j}_{3s}(\mathbf{q}), \quad (26)$$

$$\mathbf{J}_{4s} = \int dE \sum_{\mathbf{q}} \mathbf{j}_{4s}(\mathbf{q}), \quad (27)$$

with spin current densities

$$\mathbf{j}_{3s}(\mathbf{q}) = \frac{\hbar^2 k_x}{2m} \left(\psi_{3,R}^\dagger \hat{\sigma} \psi_{3,R} - \psi_{3,L}^\dagger \hat{\sigma} \psi_{3,L} \right), \quad (28)$$

$$\mathbf{j}_{4s}(\mathbf{q}) = \frac{\hbar^2 k_x}{2m} \left(\psi_{4,R}^\dagger \hat{\sigma} \psi_{4,R} - \psi_{4,L}^\dagger \hat{\sigma} \psi_{4,L} \right), \quad (29)$$

where $\hat{\sigma} = (\sigma_x, \sigma_y, \sigma_z)$ are Pauli matrices. It is convenient to recast $\hat{\sigma}$ in local orthogonal coordinates of $\mathbf{m}_B \times (\mathbf{m}_B \times \mathbf{m}_A)$, $\mathbf{m}_B \times \mathbf{m}_A$, and \mathbf{m}_B such that

$$\hat{\sigma} = \sigma_1 \mathbf{m}_B \times (\mathbf{m}_B \times \mathbf{m}_A) + \sigma_2 \mathbf{m}_B \times \mathbf{m}_A + \sigma_3 \mathbf{m}_B, \quad (30)$$

with

$$\begin{aligned} \sigma_1 &= \frac{1}{\sin \theta} \begin{pmatrix} -\sin \theta & \cos \theta e^{-i\phi} \\ \cos \theta e^{i\phi} & \sin \theta \end{pmatrix}, \\ \sigma_2 &= \frac{1}{\sin \theta} \begin{pmatrix} 0 & i e^{-i\phi} \\ -i e^{i\phi} & 0 \end{pmatrix}, \\ \sigma_3 &= \begin{pmatrix} \cos \theta & \sin \theta e^{-i\phi} \\ \sin \theta e^{i\phi} & -\cos \theta \end{pmatrix}. \end{aligned} \quad (31)$$

The STT on FM_B is equal to the difference of the spin currents on both sides of the ferromagnet,

$$\mathbf{\Gamma} = \mathbf{J}_{3s} - \mathbf{J}_{4s}, \quad (32)$$

and the STT density is

$$\boldsymbol{\tau} = \mathbf{j}_{3s} - \mathbf{j}_{4s}. \quad (33)$$

Thus, we have

$$\boldsymbol{\tau} = a_1 \mathbf{m}_B \times (\mathbf{m}_B \times \mathbf{m}_A) + a_2 \mathbf{m}_B \times \mathbf{m}_A + a_3 \mathbf{m}_B, \quad (34)$$

where

$$\begin{aligned} a_i &= \frac{\hbar^2 k_x}{2m} \left(\psi_{3,R}^\dagger \sigma_i \psi_{3,R} + \psi_{4,L}^\dagger \sigma_i \psi_{4,L} \right. \\ &\quad \left. - \psi_{3,L}^\dagger \sigma_i \psi_{3,L} - \psi_{4,R}^\dagger \sigma_i \psi_{4,R} \right), \quad (i = 1, 2, 3). \end{aligned} \quad (35)$$

First of all, we can show $a_3 = 0$ because of the particle current conservation and the absence of spin-flipping. This can be understood as follows: We first rotate \hat{z} to \mathbf{m}_B , then spinor state $\psi_{n,\alpha} = \hat{R}(\theta, \phi) \tilde{\psi}_{n,\alpha}$ where $\tilde{\psi}_{n,\alpha}$ is the electronic state *seen* along \mathbf{m}_B . Then, each spin density term $\psi_{n,\alpha}^\dagger \sigma_i \psi_{n,\alpha}$ in Eq. (35) becomes $\tilde{\psi}_{n,\alpha}^\dagger \hat{R}^\dagger(\theta, \phi) \sigma_i \hat{R}(\theta, \phi) \tilde{\psi}_{n,\alpha} = \tilde{\psi}_{n,\alpha}^\dagger \sigma_z \tilde{\psi}_{n,\alpha}$, so that spin up state (parallel to \mathbf{m}_B) and spin down state (anti-parallel to \mathbf{m}_B) are decoupled without mixing. In the absence of spin-flipping, both spin-up and spin-down particle currents are conserved. Thus, the STT projected along local magnetization \mathbf{m}_B is zero. Here we have used identity $\hat{R}^\dagger(\theta, \phi) \sigma_3 \hat{R}(\theta, \phi) = \sigma_z$. The physical consequence is that STT can only rotate the magnetization without change its magnitude.

Therefore, the STT can be divided into an in-plane (Slonczewski) term⁹ $\boldsymbol{\tau}_{\parallel} = a_1 \mathbf{m}_B \times (\mathbf{m}_B \times \mathbf{m}_A)$ and an out-of-plane (field-like) term³³ $\boldsymbol{\tau}_{\perp} = a_2 \mathbf{m}_B \times \mathbf{m}_A$. We

note that the out-of-plane torque will vanish if $t_u, t_d, r_u,$ and r_d are real. This is because all the spins of both transmitted and reflected electrons are in the same plane spanned by \mathbf{m}_A and \mathbf{m}_B under the condition, and they can only vary in this plane.

Parameters a_1 and a_2 are important to understand the spin dynamics in DSV.^{21,22} In Ref. 21, these parameters are chosen to vary continuously without geometry dependence, while they are calculated in the diffusivity transport limit in Ref. 22. To find a_1 and a_2 in our model, one needs to compute quantities

$$T_{\sigma_i}(z_1) = \frac{1}{2} \text{Tr} \left(\hat{P}_{3,R}^\dagger \sigma_i \hat{P}_{3,R} - \hat{P}_{3,L}^\dagger \sigma_i \hat{P}_{3,L} - \hat{P}_{4,R}^\dagger \sigma_i \hat{P}_{4,R} + \hat{P}_{4,L}^\dagger \sigma_i \hat{P}_{4,L} \right), \quad (i = 1, 2), \quad (36)$$

since $a_i = T_{\sigma_i}(z_1) (\hbar^2 k_x) / m$, ($i = 1, 2$). Perform the same averaging procedure as we did on the charge current early, one finds

$$\langle T_{\sigma_i} \rangle = \sum_{l_i=1}^{s_i} \text{Res} \left(\frac{T_{\sigma_i}(z_1)}{z_1}; z_{1,l_i} \right), \quad (i = 1, 2), \quad (37)$$

where z_{1,l_i} is the l_i -th pole of function $T_{\sigma_i}(z_1)/z_1$ inside the unit circle in the complex plane with s_i the corresponding total pole number.

Since only region b contributes to the spin current,^{9,28} one has $\langle a_i \rangle = \frac{\hbar}{e} \langle T_{\sigma_i} \rangle J_b$, ($i = 1, 2$). Thus the average STT on the free magnetic layer is

$$\mathbf{\Gamma} = g_1(\theta) \frac{\hbar}{e} J_e \mathbf{m}_B \times (\mathbf{m}_B \times \mathbf{m}_A) + g_2(\theta) \frac{\hbar}{e} J_e \mathbf{m}_B \times \mathbf{m}_A, \quad (38)$$

with scalar functions

$$g_i(\theta) = \frac{\langle T_{\sigma_i} \rangle}{J_a / J_b + \langle T_e \rangle}, \quad (i = 1, 2). \quad (39)$$

The STT $\mathbf{\Gamma}$ consists of two terms. The first one is Slonczewski torque $\mathbf{\Gamma}_{\parallel} = g_1(\theta) \frac{\hbar}{e} J_e \mathbf{m}_B \times (\mathbf{m}_B \times \mathbf{m}_A)$. And the second one is field-like torque $\mathbf{\Gamma}_{\perp} = g_2(\theta) \frac{\hbar}{e} J_e \mathbf{m}_B \times \mathbf{m}_A$.

The general analytical forms of $g_1(\theta)$ and $g_2(\theta)$ are difficult to find because of the complicated residue calculations in Eqs. (18) and (37). However, they can be numerically evaluated for any given material with definite material parameters $t_u, t_d, r_u,$ and r_d . In Fig. 3, we present the numerical calculations of the magnitude of Slonczewski torque $\Gamma_{\parallel} = -g_1(\theta) \frac{\hbar}{e} J_e \sin \theta$ per unit current versus angle θ at polarization coefficient $P = 0.6$ under three different conditions, which shows that different transmission probabilities have strong impact on the torque and may change the sign of the torque. Similar sign reversal of STT is demonstrated in usual spin valve.²⁹

Here, in order to directly compare our results in DSV with Slonczewski's result in conventional spin valve,⁹ let us consider the case of ideal FM_B, i.e., $t_u = 1$ and $t_d = 0$ ($r_u = 0, r_d = 1$). After some algebras, we obtain

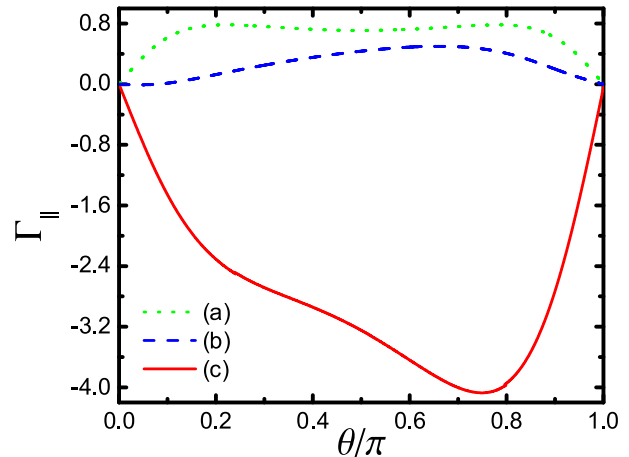


FIG. 3: (Color online) Slonczewski torque Γ_{\parallel} versus θ for polarization $P = 0.6$ under three different conditions: (a) $t_u = 1$ and $t_d = 0$; (b) $|t_u|^2 = 0.99$ and $|t_d|^2 = 0.1$; and (c) $|t_u|^2 = 0.84$ and $|t_d|^2 = 0.17$. The unit of torque is $\frac{\hbar}{e} J_e$.

$T_{\sigma_1} = \frac{1}{4}(z_1 + z_1^* - 2)$ and $T_{\sigma_2}(z_1) = -\frac{i}{4}(z_1 - z_1^*)$. The averaged values are then

$$\langle T_{\sigma_1} \rangle (t_u = 1, t_d = 0) = -\frac{1}{2}, \quad (40)$$

$$\langle T_{\sigma_2} \rangle (t_u = 1, t_d = 0) = 0. \quad (41)$$

Thus we get the scalar g -functions

$$g_1(\theta) = \frac{-1}{-3 + (1+P)^3 / (2P^{3/2}) - (\mathbf{m}_A \cdot \mathbf{m}_B)^2}, \quad (42)$$

$$g_2(\theta) = 0, \quad (43)$$

which show that only the Slonczewski torque exists in the ideal DSV. The absence of any layer-thickness dependence in Eq. (42) results from the phase average across sufficiently thick normal metal layers. The values of $g_1(\theta = 0, \pi)$ are crucial to evaluate the threshold current density J_e^* needed for magnetization reversal of the free layer since $J_e^* \propto 1/g_1(\theta = 0, \pi)$.¹⁶

Figure 4 is the magnitude of STT per unit current as a function of angle θ for various polarization P in ideal DSV. The STT is symmetric against $\pi/2$ due to the contributions from both fixed magnetic layers, which is different from the result in conventional spin valve.^{9,28,29} For polarization coefficient $P < 1$ it generally vanishes at $\theta = 0$ and $\theta = \pi$ (shown in Fig. 4). However, if $P = 1$, the torque is singular at $\theta = 0$ and π . The divergence can be understood mathematically and from a physics viewpoint. Mathematically, the singularities at $\theta = 0$ and π are due to the factor of $g_1 = -(\sin \theta)^{-2}$ when $P = 1$. Physically this is the consequence of perfect spin filter. In our model, every electron transfers its angular momentum to local magnetization when it impinges the interface of magnetic layer whose magnetization is not parallel to its spin.⁹ Meanwhile, the STT per unit current is defined

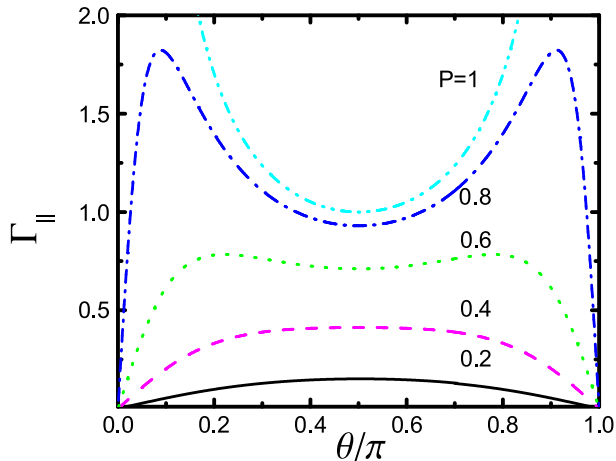


FIG. 4: (Color online) Slonczewski torque Γ_{\parallel} versus angle θ for various polarization P in the ideal case where all FMs are perfect polarizers. The unit of torque is $\frac{\hbar}{e}J_e$.

as the spin transfer per transmitted electron.⁹ However, in the case of $\theta = 0$ or $\theta = \pi$, perfect spin filter does not allow any electron transmitting through the DSV, which leads to a zero electron transmission and results in the divergence. The above argument can also be applied to the STT divergence at $\theta = \pi$ in traditional spin valve in the original paper by Slonczewski.⁹ Nevertheless, we find that the total STT $\mathbf{\Gamma} = -\frac{1}{2}\frac{\hbar}{e}J_b\mathbf{m}_B \times (\mathbf{m}_B \times \mathbf{m}_A)$ if $P = 1$, does not have such singularities.

Finally, we would like to compare the magnitude of STT in our DSV with that obtained in traditional spin valve.²⁸ In Ref. 28, Krstajić *et al.* calculated the g -function in spin valve

$$g_1^*(\theta) = \frac{-1}{-4 + (1 + P)^3 (3 + \mathbf{m}_A \cdot \mathbf{m}_B) / (4P^{3/2})}, \quad (44)$$

which is the same as the Slonczewski's result in Ref. 9.

We plot the ratio $g_1(\theta)/g_1^*(\theta)$ as a function of angle θ for various polarization P in Fig. 5. One can see that the STT is largely enhanced when θ is acute, but approaches to that in usual spin valve when $\theta > \pi/2$. Namely, the enhancement value sensitively depends on both the orientation of free layer and the polarization degree of electrons. Under small tilted angle θ and large polarization P , the enhancement ratio is dramatic, which will substantially lower the required threshold current density for magnetization switching. For instance, $g_1/g_1^* = 11.9$ if $\theta = \frac{\pi}{6}$ and $P = 0.8$. While the enhancement ratio approaches to 1 (red dash line shown in Fig. 5) when θ is close to π . The reason is that there is no difference between a DSV and a usual spin valve when layers FM_A and FM_B are antiparallely aligned, since FM_C would not reflect electrons coming out of FM_B in such case. The results are qualitatively consistent with Fuchs *et al.*'s experiment³⁴ which shows that the reduction of threshold current switching FM_B from parallel to antiparallel, with respect to FM_A , is substantial, while it is only of modest size from antipar-

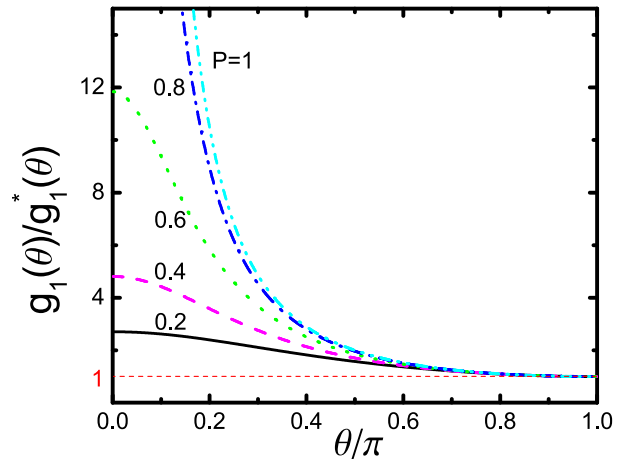


FIG. 5: (Color online) Spin transfer torque enhancement ratio $g_1(\theta)/g_1^*(\theta)$ versus θ for various polarization P in the ideal case where all FMs are perfect polarizers.

allel to parallel in DSV compared to that in conventional spin valve.

From the qualitative physical picture and quantum mechanical calculations, we conclude that STT can be greatly enhanced in DSV compared to that in spin valve structure in the ballistic regime without spin accumulations. The findings of the physics behind and the analytical formula of STT in this emerging geometry should be interesting for both theoretical^{21,22} and experimental^{34,35} concerns. Micromagnetic simulation based on our new g -function (Eq. (42)) and Landau-Lifshitz-Gilbert (LLG) equation³⁶ will be a direction of future research. The behavior of STT in asymmetric DSV when the widths of two NMs are different, i.e., $l_A \neq l_B$, is also an interesting issue for further investigation.

Although the advantage of STT enhancement is unambiguously demonstrated in our results, the accuracy of the analytical formula still needs experimental confirmation. We suggest to use a recently developed technique called spin-transfer-driven ferromagnetic resonance (ST-FMR)³⁷ to measure the angular dependence of the STT in DSV.

V. SUMMARY

In conclusion, we derive the STT acting on the free magnetic layer in a DSV structure in the ballistic regime. A full-quantum mechanics description of the STT is presented, which is valid for nanoscale DSVs where both the electron mean-free path and the spin-flip relaxation length are larger than the thickness of the spacers.³⁸ Using a quasi-one-dimensional model and within the Slonczewski's approach, we obtained the analytical form of the STT when all magnetic layers are perfect polarizers. Similar to the results in the diffusive regime, the STT is

dramatically enhanced in comparison to that in a conventional spin valve although no spin accumulation exists at the magnetic-nonmagnetic interfaces. Depending on the orientation of free magnetic layer and the polarization degree of electrons, the STT can be enhanced by a factor of a few tens. Our analytical g -function provides a theoretical base for the micromagnetic simulation of the spin dynamics in DSV. The general cases when transmission and reflection probabilities of free layer are different from zero or one are also numerically calculated, which shows that the sign of the torque may change under different transmission probabilities. These results should be useful for the switching current reduction in magnetization

reversal.

ACKNOWLEDGMENTS

This work is supported by Hong Kong RGC grants (#603007, 603508, 604109 and HKU10/CRF/08-HKUST17/CRF/08). X.R.W. would like to acknowledge the hospitality of Kavli Institute for Theoretical Physics China, CAS. Z.Z.S. thanks the Alexander von Humboldt Foundation (Germany) for a grant.

-
- ¹ J.A. Katine, F.J. Albert, R.A. Buhrman, E.B. Myers, and D.C. Ralph, *Phys. Rev. Lett.* **84**, 3149 (2000).
- ² J. Grollier, V. Cros, A. Hamzic, J.M. George, H. Jaffrès, A. Fert, G. Faini, J.B. Youssef, and H. Legall, *Appl. Phys. Lett.* **78**, 3663 (2001).
- ³ K. Xia, P.J. Kelley, G.E.W. Bauer, A. Brataas, and I. Turek, *Phys. Rev. B* **65**, 220504(R) (2002).
- ⁴ S. Urazhdin, N.O. Birge, W.P. Pratt, and J. Bass, *Phys. Rev. Lett.* **91**, 146803 (2003).
- ⁵ M. Tsoi, J.Z. Sun, and S.S.P. Parkin, *Phys. Rev. Lett.* **93**, 036602 (2004).
- ⁶ T.Y. Chen, S.X. Huang, C.L. Chien, and M.D. Stiles, *Phys. Rev. Lett.* **96**, 207203 (2006).
- ⁷ Y. Zhou, C.L. Zha, S. Bonetti, J. Persson, and J. Åkerman, *Appl. Phys. Lett.* **92**, 262508 (2008).
- ⁸ X. Chen, Q.R. Zheng, and G. Su, *Phys. Rev. B* **78**, 104410 (2008).
- ⁹ J.C. Slonczewski, *J. Magn. Magn. Mater.* **159**, L1 (1996).
- ¹⁰ L. Berger, *Phys. Rev. B* **54**, 9353 (1996).
- ¹¹ Z.Z. Sun and X.R. Wang, *Phys. Rev. B* **71**, 174430 (2005); **73**, 092416 (2006); **74**, 132401 (2006).
- ¹² X.R. Wang, P. Yan, J. Lu, and C. He, *Ann. Phys. (N. Y.)* **324**, 1815 (2009); X.R. Wang, P. Yan, and J. Lu, *Europhys. Lett.* **86**, 67001 (2009).
- ¹³ A. Yamaguchi, T. Ono, S. Nasu, K. Miyake, K. Mibu, and T. Shinjo, *Phys. Rev. Lett.* **92**, 077205 (2004).
- ¹⁴ M. Hayashi, L. Thomas, C. Rettner, R. Moriya, Y.B. Bazaliy, and S.S.P. Parkin, *Phys. Rev. Lett.* **98**, 037204 (2007).
- ¹⁵ P. Yan and X.R. Wang, *Phys. Rev. B* **80**, 214426 (2009); *Appl. Phys. Lett.* **96**, 162506 (2010).
- ¹⁶ X.R. Wang and Z.Z. Sun, *Phys. Rev. Lett.* **98**, 077201 (2007); X.R. Wang, P. Yan, J. Lu, and C. He, *Europhys. Lett.* **84**, 27008 (2008).
- ¹⁷ H.Z. Lu and S.Q. Shen, *Phys. Rev. B* **80**, 094401 (2009).
- ¹⁸ M. Hatami, G.E.W. Bauer, Q. Zhang, and P.J. Kelly, *Phys. Rev. Lett.* **99**, 066603 (2007).
- ¹⁹ Z. Yuan, S. Wang, and K. Xia, *Solid State Commun.* **150**, 548 (2010).
- ²⁰ L. Berger, *J. Appl. Phys.* **93**, 7693 (2003).
- ²¹ C.Y. You, *J. Appl. Phys.* **107**, 073911 (2010).
- ²² P. Baláz, M. Gmitra, and J. Barnaś, *Phys. Rev. B* **80**, 174404 (2009).
- ²³ T. Valet and A. Fert, *Phys. Rev. B* **48**, 7099 (1993).
- ²⁴ J. Xiao, A. Zangwill, and M.D. Stiles, *Phys. Rev. B* **70**, 172405 (2004).
- ²⁵ M.D. Stiles and A. Zangwill, *Phys. Rev. B* **66**, 014407 (2002).
- ²⁶ D. Waldron, P. Haney, B. Larade, A. MacDonald, and H. Guo, *Phys. Rev. Lett.* **96**, 166804 (2004).
- ²⁷ A. Brataas, Y.V. Nazarov, and G.E.W. Bauer, *Phys. Rev. Lett.* **84**, 2481 (2000); A. Brataas, Y.V. Nazarov, and G.E.W. Bauer, *Eur. Phys. J. B* **22**, 99 (2001).
- ²⁸ P.M. Krstajić, M. Keller, and F.M. Peeters, *Phys. Rev. B* **77**, 174428 (2008).
- ²⁹ X. Waintal, E.B. Myers, P.W. Brouwer, and D.C. Ralph, *Phys. Rev. B* **62**, 12317 (2000).
- ³⁰ J. Xiao and G.E.W. Bauer, *Phys. Rev. B* **77**, 224419 (2008).
- ³¹ M. Gmitra and J. Barnaś, *Appl. Phys. Lett.* **89**, 223121 (2006).
- ³² M.D. Stiles, *J. Appl. Phys.* **79**, 5805 (1996).
- ³³ S. Zhang, P.M. Levy, and A. Fert, *Phys. Rev. Lett.* **88**, 236601 (2002).
- ³⁴ G.D. Fuchs, I.N. Krivorotov, P.M. Braganca, N.C. Emley, A.G.F. Garcia, D.C. Ralph, and R.A. Buhrman, *Appl. Phys. Lett.* **86**, 152509 (2005).
- ³⁵ M. Watanabe, J. Okabayashi, H. Toyao, T. Yamaguchi, and J. Yoshino, *Appl. Phys. Lett.* **92**, 082506 (2008).
- ³⁶ T.L. Gilbert, *IEEE Trans. Magn.* **40**, 3443 (2004).
- ³⁷ J.C. Sankey, P.M. Braganca, A.G.F. Garcia, I.N. Krivorotov, R.A. Buhrman, and D.C. Ralph, *Phys. Rev. Lett.* **96**, 227601 (2006); J.C. Sankey, Y.T. Cui, J.Z. Sun, J.C. Slonczewski, R.A. Buhrman, and D.C. Ralph, *Nature Phys.* **4**, 67 (2008).
- ³⁸ F.J. Jedema, M.S. Nijboer, A.T. Filip, and B.J. van Wees, *Phys. Rev. B* **67**, 085319 (2003).